Matched optical vortices of slow light using a tripod coherently prepared scheme

Hamid R. Hamedi [1,*] Ite A. Yu [2,3] and Emmanuel Paspalakis [4,†]

[1]*Institute of Theoretical Physics and Astronomy, Vilnius University, Saulėtekio 3, Vilnius LT-10257, Lithuania*

[2]*Department of Physics, National Tsing Hua University, Hsinchu 30013, Taiwan*

[3]*Center for Quantum Science and Technology, National Tsing Hua University, Hsinchu 30013, Taiwan*

[4]*Materials Science Department, School of Natural Sciences, University of Patras, Patras 265 04, Greece*

(Received 30 July 2023; accepted 13 November 2023; published 30 November 2023)

This paper explores the propagation of optical vortices of slow light inside a four-level tripod atomic light-matter coupling system. Initially, the system is prepared in a coherent superposition of two out of the three lower levels by, for example, coherent population trapping, while the third lower state remains unoccupied. The unoccupied state is coupled to a strong control laser field with a constant Rabi frequency, lacking orbital angular momentum (OAM). Simultaneously, one of the remaining lower states interacts with a weak vortex beam. The third lower state has no initial coupling to any field. This arrangement effectively closes the level transitions, resulting in a phase-dependent configuration. By solving the Maxwell-Schrödinger equations, we provide analytical evidence that the application of a strong control field can generate an additional optical vortex of slow light. This vortex possesses the same OAM as the incident vortex beam. Furthermore, we explore the matching of optical vortices at different propagation distances, contingent upon the intensity of the control field. Additionally, our analysis extends to a more complex five-level tripod and Λ scheme, where we introduce two additional strong control fields to prepare the atoms in a coherent superposition of two lower levels.

DOI: 10.1103/PhysRevA.108.053719

I. INTRODUCTION

In recent years, slow light has witnessed a surge of activity, showcasing remarkable advancements and discoveries. A multitude of studies have delved into this intriguing field [1–5]. Moreover, investigations into stored light [6–9], alongside stationary light [10–13], have contributed significantly to our understanding. One particularly groundbreaking achievement involves the demonstration of a resonant weak pulse of light, commonly referred to as the probe light, exhibiting an extraordinary ability to propagate at significantly reduced speeds. In fact, velocities as low as several tens of meters per second have been observed in atomic media driven by a more powerful control laser beam [1]. The control laser's application induces a transformative effect on the resonant and initially opaque medium, leading to a phenomenon known as electromagnetically induced transparency (EIT) [14–17]. This interplay between the two beams establishes a unique configuration that fosters efficient coupling between atoms and light.

The implications of slow light extend far beyond theoretical curiosity, finding practical applications in various domains. Notably, slow light serves as a valuable tool in reversible quantum memories [14,18], where the ability to decelerate light facilitates the storage and retrieval of delicate quantum information. Researchers have also explored the realm of moving media [19,20], where the utilization of slow light opens up new possibilities for rotational sensing devices. These devices leverage the controlled deceleration of light to enable precise measurements and enhance sensing capabilities, ushering in a new era of technological advancements.

The realm of slow light further expands its horizons through the utilization of orbital angular momentum (OAM) [21–23]. The incorporation of OAM introduces a different dimension for manipulating and harnessing the potential of slow light, particularly in the fields of quantum computation and quantum information storage [24,25].

When spatially dependent beams, characterized by their OAM, interact with matter waves, intriguing effects come into play, offering a plethora of exciting possibilities [26–39]. The introduction of OAM as an additional degree of freedom in manipulating optical information has sparked considerable interest, as it unveils avenues for precisely controlling and manipulating the flow of light. Among the various effects that arise from the interaction of vortex beams with matter waves, the exchange of optical vortices has attracted considerable interest [4,26–28,31,33,40–42]. This phenomenon becomes particularly intriguing due to the additional degree of freedom introduced by OAM, enabling the manipulation of optical information in unprecedented ways.

Previous studies have predominantly focused on the interaction of optical vortices with atomic structures under the conditions of EIT, where atoms are initially in their ground states [26,41]. Specifically, a four-level atom-light coupling scheme of the tripod type has been proposed to facilitate the transfer of optical vortices between different frequencies during the storage and retrieval of the probe field [40]. However, the exchange of optical vortices within non-closed-loop

*hamid.hamedi@tfai.vu.lt

†paspalak@upatras.gr

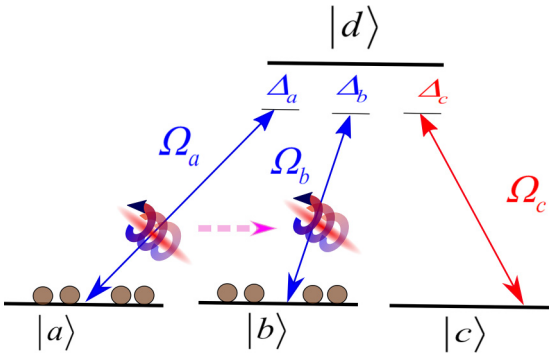

FIG. 1. The level structure of a four-level atom-light coupling scheme with a tripod configuration.

$(n+1)$-level schemes, consisting of n ground states and one excited state, has recently been demonstrated under the condition of weak atom-light interaction [43,44] in coherently prepared phaseonium atomic media [27]. In such configurations, the atoms are prepared in a coherent superposition of all n lower levels, enabling the incident vortex beam to create $(n-1)$ new optical vortices with the same vorticity as the incident beam. Yet, these optical vortices are not associated with slow light.

In order to transfer optical vortices of slow light, a different scenario is explored in this paper. Consider a four-level tripod system, as illustrated in Fig. 1, which is prepared in a superposition of two (out of three) lower states $|a\rangle$ and $|b\rangle$, while the third lower state $|c\rangle$ remains unoccupied. The initially unoccupied lower state $|c\rangle$ is coupled by a strong control laser field with a constant Rabi frequency (without OAM), while one of the other two lower states $|a\rangle$ interacts with a weak vortex beam. The other lower state $|b\rangle$ is not initially coupled to any field. Under this arrangement, a new vortex field is generated by the weak field with OAM. It becomes possible for both the initially weak field and the generated vortex fields to propagate as slow light, controlled by the influence of the control field. This configuration opens up avenues for transferring optical vortices using slow light without the need for storage and retrieval of the probe field [40]. It introduces exciting prospects for manipulating and controlling optical information with tailored vortex beams.

II. THE MODEL

A. Hamiltonian and system

Consider the arrangement depicted in Fig. 1, referred to as the tripod configuration. This configuration comprises three distinct lower states, denoted as $|a\rangle$, $|b\rangle$, and $|c\rangle$, which are interconnected to an excited state through the influence of three laser fields. Each laser field is characterized by its respective Rabi frequency: Ω_a, Ω_b, and Ω_c. The excited state $|d\rangle$ undergoes decay to the lower states at a rate of Γ. By employing the rotating wave and dipole approximations, the interaction Hamiltonian governing the dynamics of this system can be expressed as follows:

$$H = \sum_{s=a,b,c} \Omega_s e^{-i\Delta_s t}|s\rangle\langle d| + \text{H.c.} \tag{1}$$

The detunings, denoted as $\Delta_s = \omega_d - \omega_s - \overline{\omega}_s$, quantify the deviation from resonance between the excited state $|d\rangle$ and the lower states $|s\rangle$ (where s can be a, b, or c). Here, ω_s represents the energy of the lower state $|s\rangle$, ω_d represents the energy of the excited state $|d\rangle$, and $\overline{\omega}_s$ represents the angular frequency of the corresponding laser field.

The system's description can be formulated using a state vector, which is expressed as a sum of atomic basis states multiplied by their respective time-dependent amplitudes, denoted as V_i:

$$\begin{aligned}\Psi(t) = V_a|a\rangle + V_b e^{-i(\Delta_b-\Delta_a)t}|b\rangle \\ + V_c e^{-i(\Delta_c-\Delta_a)t}|c\rangle + V_d e^{i\Delta_a t}|d\rangle.\end{aligned} \tag{2}$$

By substituting Eqs. (1) and (2) into the Schrödinger equations, we can derive the equations for the probability amplitudes:

$$\frac{\partial}{\partial t}\boldsymbol{V} = -i\boldsymbol{M}\boldsymbol{V}, \tag{3}$$

where

$$\boldsymbol{M} = \begin{bmatrix} 0 & 0 & 0 & \Omega_a \\ 0 & \Delta_a-\Delta_b & 0 & \Omega_b \\ 0 & 0 & \Delta_a-\Delta_c & \Omega_c \\ \Omega_a^* & \Omega_b^* & \Omega_c^* & \Delta_a - i\Gamma \end{bmatrix} \tag{4}$$

and

$$\boldsymbol{V} = \begin{bmatrix} V_a \\ V_b \\ V_c \\ V_d \end{bmatrix}. \tag{5}$$

At the initial stage, the tripod system is prepared in a superposition of two lower levels, namely, $|a\rangle$ and $|b\rangle$. The wave function at this initial time is given by

$$\Psi(0) = \cos\theta|a\rangle + \sin\theta|b\rangle, \tag{6}$$

where θ represents a preparation angle. Such a state can be prepared via coherent methods such as coherent population trapping (CPT) [45,46], a transverse magnetic field, or using the fractional or partial stimulated Raman adiabatic passage (STIRAP) in which only a controlled fraction of the population is transferred to the target state [47]. In this scenario, we assume that the two laser fields, characterized by the detunings $\Delta_a = \Delta_b = \Delta$, are in two-photon resonance. Additionally, we consider a weak atom-light interaction, where the magnitudes of the Rabi frequencies are much smaller than the Rabi frequency associated with field c, i.e., $|\Omega_a|, |\Omega_b| \ll |\Omega_c|, \Gamma$. Under these assumptions, we can obtain an approximate solution for Eq. (3) as follows:

$$\begin{bmatrix} V_a \\ V_b \\ V_c \\ V_d \end{bmatrix} = \begin{bmatrix} \cos\theta \\ \sin\theta \\ -\frac{\Omega_c V_d}{\Delta-\Delta_c} \\ -\frac{\Omega_a^*\cos\theta+\Omega_b^*\sin\theta}{\delta-i\Gamma} \end{bmatrix}, \tag{7}$$

where $\delta = \Delta - |\Omega_c|^2/(\Delta-\Delta_c)$. Equations (6) and (7) introduce a coherence between states $|a\rangle$ and $|b\rangle$ in the system, i.e.,

$\rho_{ab} = V_a V_b^* = \cos\theta \sin\theta$ is not zero anymore, where ρ is the density-matrix operator.

Before proceeding to the next section, we will demonstrate the practical implementation of the tripod setup within the context of utilizing Rb-87 atoms as an illustrative example. First, we state $|a\rangle$ represented as $|5S_{1/2}, F = 1, m = -1\rangle$. Moving on, state $|b\rangle$ corresponds to $|5S_{1/2}, F = 1, m = +1\rangle$, while state $|c\rangle$ is denoted as $|5S_{1/2}, F = 2, m = 1\rangle$ (or similarly, $|5S_{1/2}, F = 2, m = -1\rangle$). Finally, state $|d\rangle$ is defined as $|5P_{3/2}, F = 1, m = 0\rangle$. The probe fields Ω_a and Ω_b have the σ_+ and σ_- polarizations, respectively, while the coupling field has the σ_- (or similarly σ_+) polarization. All three fields can propagate in the same directions to greatly eliminate the Doppler effect, which degrades the EIT-related phenomena, even in a Doppler-broadened medium [48,49]. To initiate the scheme, one may apply an optical pumping field, which induces the transition from $|5S_{1/2}, F = 1, m = 0\rangle$ to $|5P_{3/2}, F = 0, m = 0\rangle$. Consequently, all the population initially residing in the ground level with $F = 1$ will accumulate in the Zeeman states with $m = -1$ and $m = 1$. Efficiently emptying the population in $|5S_{1/2}, F = 1, m = 0\rangle$ eliminates the need to consider probe a and b transitions from this state to $|5P_{3/2}, F = 1, m = 1\rangle$ and $|5P_{3/2}, F = 1, m = -1\rangle$ [50], respectively.

B. Absorption and dispersion characteristics

To show that the present system is capable of the transfer of vortices of slow light, the closed linkage between fields Ω_a and Ω_b is discussed in this section. The closed linkage will be revealed by the phenomenon that when fields Ω_a and Ω_b are both present at the input, the outcome will depend on the relative phase between them. By introducing the Rabi frequencies as follows: $\Omega_a = |\Omega_a| e^{i\Phi_a}$, $\Omega_b = |\Omega_b| e^{i\Phi_b}$, and $\Omega_c = |\Omega_c| e^{i\Phi_c}$, where Φ_a, Φ_b, and Φ_c represent the respective phase information carried by each field a, b, and c, the equations for the susceptibilities of weak probe fields can be expressed as

$$\chi_a(\Delta) = \frac{-4\pi N|\mu|^2}{\Omega_a} V_a V_d^* = 4\pi N|\mu|^2 \frac{\cos^2\theta + \frac{\Omega_b}{\Omega_a} e^{-i\Phi} \sin\theta \cos\theta}{\delta + i\Gamma}, \quad (8)$$

$$\chi_b(\Delta) = \frac{-4\pi N|\mu|^2}{\Omega_b} V_b V_d^* = 4\pi N|\mu|^2 \frac{\frac{\Omega_a}{\Omega_b} e^{i\Phi} \sin\theta \cos\theta + \sin^2\theta}{\delta + i\Gamma}. \quad (9)$$

We assume that the dipole moments are equal for both transitions, represented as $\mu_{ad} = \mu_{bd} = \mu$. Additionally, the relative phase between probe fields Ω_a and Ω_b is denoted as $\Phi = \Phi_a - \Phi_b$, and N represents the density of the atomic medium. The imaginary and real parts of $\chi_a(\Delta)$ and $\chi_b(\Delta)$ correspond to the absorption and dispersion of the weak fields Ω_a and Ω_b, respectively. By preparing the system in the superposition state described in Eq. (6), the transitions can be closed, resulting in the generation of phase-dependent dark states. These dark states, in turn, give rise to phase-dependent optical effects.

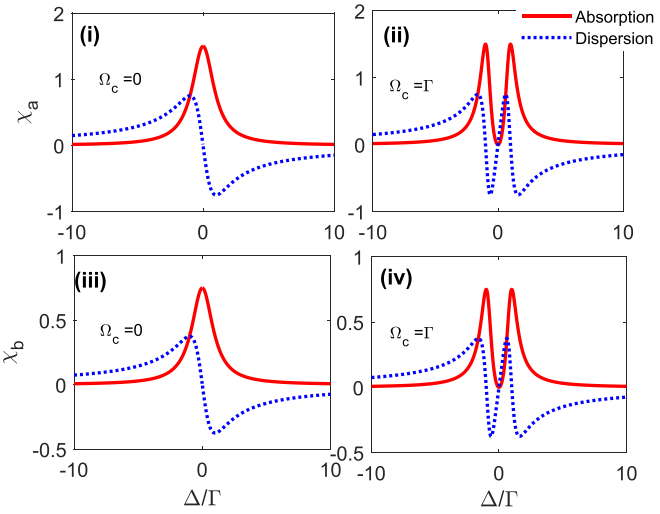

FIG. 2. The imaginary (solid) and real (dotted) parts of susceptibilities $\chi_a(\Delta)$ (top two subplots) and $\chi_b(\Delta)$ (bottom two subplots) in units of $4\pi N|\mu|^2$ versus Δ/Γ. Two cases are considered: $\Omega_c = 0$ (left subplots) and $\Omega_c = \Gamma$ (right subplots). The parameters utilized in these plots are $\Delta_c = 0$, $\Omega_a = 0.1\Gamma$, $\Omega_b = 0.2\Gamma$, and $\theta = \pi/4$.

Figure 2 shows the real (dashed) and imaginary (solid) part of susceptibilities χ_a and χ_b against Δ/Γ for $\Omega_c = 0$ and $\Omega_c = \Gamma$, when $\Delta_c = 0$, $\Omega_a = 0.1\Gamma$, $\Omega_b = 0.2\Gamma$, and $\theta = \pi/4$. It can be seen that when the control field is switched off ($\Omega_c = 0$), both fields a and b experience strong absorption around resonance while the light pulses propagate with superluminality (the slope of dispersion is negative around line center). Switching on the control field results in a dip in resonance, leading to suppression of the absorption effects (transparency). In such a situation, slow light is dominant in the medium as the slope of dispersion converted to positive at $\Delta = 0$ for both weak fields. In the absence of the control field, the system reduces to a simpler single Λ scheme, driven solely by two weak probe fields. However, when the control field is introduced into the third transition of the tripod scheme ($|c\rangle \leftrightarrow |d\rangle$), the system can be seen as two individual Λ schemes. In each of these schemes, there is a weak probe field and a strong control field. The strong control field, denoted as Ω_c, now interacts with the Λ atoms, effectively suppressing probe field absorption at both transitions and simultaneously reducing the group velocity of light [14]. Note that this was not possible for the tripod scheme where all three lower states are coherently prepared and illuminated by three weak probe fields [27].

Figure 3 depicts the influence of the relative phase information carried by the probe fields on the behavior of susceptibilities. It is evident that the relative phase plays a significant role in manipulating the results. Specifically, when setting Φ equal to π, a gain doublet is observed for field a [subplot ii in Fig. 3(a)]. The dispersion slope exhibits a negative trend within the gain doublet window, indicating superluminal light propagation. Conversely, the dispersion slope takes on a positive character within the regions where the gain is maximized, signifying subluminal light propagation. On the other hand, an absorption doublet associated with subluminality occurs for field b under the same conditions [subplot ii

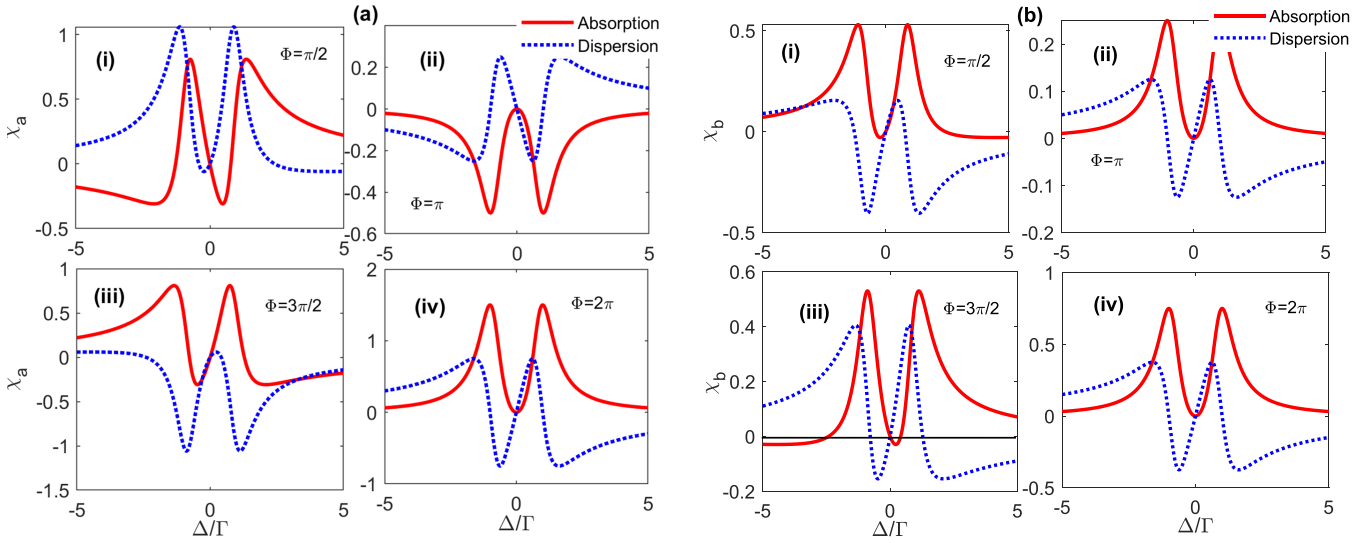

FIG. 3. The imaginary (solid) and real (dotted) parts of susceptibilities $\chi_a(\Delta)$ (a) and $\chi_b(\Delta)$ (b) in units of $4\pi N|\mu|^2$ versus Δ/Γ. The plots showcase the behavior for different relative phase values: $\Phi = \pi/2, \pi, 3\pi/2$, and 2π. Here, we set $\Omega_c = \Gamma$ while the remaining parameters remain the same as in Fig. 2. The solid horizontal line in (b iii) serves as the boundary between zero absorption and gain, effectively separating the two.

in Fig. 3(b)]. Moreover, the system exhibits amplification for field Ω_a when Φ is set to $\pi/2$ [see subplot i in Fig. 3(a)], while amplification for field Ω_b occurs when Φ is equal to $3\pi/2$, as seen in subplot iii in Fig. 3(b). These observations highlight the profound impact of the relative phase on the characteristics of the system and its ability to control and manipulate the optical effects observed in the probe fields.

Therefore, a closed linkage between the atomic excitation when dealing with weak fields prepared coherently in the superposition state Eq. (6) leads to phase-dependent population dynamics. This characteristic, which is absent in a simple Λ or tripod scheme operating under EIT conditions [4,40,51], will play a pivotal role in the subsequent section. In the next section, we will leverage this phase-coherent process to analyze the spatially dependent propagation dynamics of weak pulse beams carrying OAM.

C. Optical vortices of slow light

The propagation equation for the weak laser fields can be described by the Maxwell equation in the slowly varying amplitude and phase approximation,

$$\frac{\partial}{\partial z}\begin{bmatrix}\Omega_a\\ \Omega_b\end{bmatrix} + c^{-1}\frac{\partial}{\partial t}\begin{bmatrix}\Omega_a\\ \Omega_b\end{bmatrix} = i\zeta\begin{bmatrix}V_a\\ V_b\end{bmatrix}V_d^*, \tag{10}$$

where $\zeta = \frac{2\pi N|\mu|^2\overline{\omega}_s}{c}$. In this equation, we have neglected the diffraction terms containing the transverse derivatives [26–28]. By substituting the given propagation equation into the Maxwell equation (10), the equation is transformed as follows:

$$\frac{\partial}{\partial z}\begin{bmatrix}\Omega_a\\ \Omega_b\end{bmatrix} = -i\boldsymbol{K}\begin{bmatrix}\Omega_a\\ \Omega_b\end{bmatrix}, \tag{11}$$

where the matrix K is defined as

$$\boldsymbol{K} = \wp\begin{bmatrix}\cos^2\theta & \sin\theta\cos\theta\\ \sin\theta\cos\theta & \sin^2\theta\end{bmatrix}, \tag{12}$$

with $\wp = \zeta\frac{1}{i\Gamma+\Delta-\frac{|\Omega_c|^2}{\Delta-\Delta_c}}$. The matrix K captures the influence of the phase angle θ on the propagation of the fields Ω_a and Ω_b.

Taking into account the initial conditions, where the field Ω_a at $z = 0$ is given by $\Omega_a(0) = \Omega_{a0}(\frac{r}{w})^{|l|}e^{-r^2/w^2}e^{il\phi}$ (r describes a cylindrical radius, w is a beam waist, l is OAM number, and ϕ is azimuthal angle) and the field Ω_b is initially set to zero, $\Omega_b(z) = 0$, we can apply these initial conditions to the propagation equation, giving

$$\begin{bmatrix}\Omega_a(z)\\ \Omega_b(z)\end{bmatrix} = \Omega_{a0}\left(\frac{r}{w}\right)^{|l|}e^{-r^2/w^2}e^{il\phi}\begin{bmatrix}\cos^2\theta e^{-i\wp z} + \sin^2\theta\\ \sin\theta\cos\theta(e^{-i\wp z}-1)\end{bmatrix}. \tag{13}$$

The coherence between the incident beam and the generated beam is evident, as the generated beam b acquires the same phase as beam a. This indicates that the vortex carried by the incident beam a is transferred to the generated beam b. Through a coherent internal generation process, a medium prepared coherently in two of the three lower levels can generate an additional optical vortex from the applied fields. Figure 4 illustrates the dependence of the dimensionless intensities of the light fields, $|\Omega_a(z)|^2/|\Omega_a(0)|^2$ (solid line) and $|\Omega_b(z)|^2/|\Omega_a(0)|^2$ (dashed-dotted line), as given in Eq. (13), on the distance ζz for different values of the control field Ω_c. The four cases considered are (i) $\Omega_c = 0.2\Gamma$, (ii) $\Omega_c = 0.6\Gamma$, (iii) $\Omega_c = \Gamma$, and (iv) $\Omega_c = 1.5\Gamma$. These simulations are conducted with a nonzero but exceedingly small two-photon detuning, i.e., $\Delta = 0.1\Gamma$. This choice is driven by two pivotal reasons. Firstly, in realistic systems, relaxation or decoherence is always present, and the decoherence rate is never precisely zero. On the other hand, perfect EIT, characterized by a zero two-photon detuning and zero decoherence rate, inhibits any probe transition, which, in turn, precludes vortex transfer. In our case, we consider an idealized model with zero decoherence rates. Consequently, introducing a nonzero two-photon detuning is necessary to deviate from perfect EIT conditions

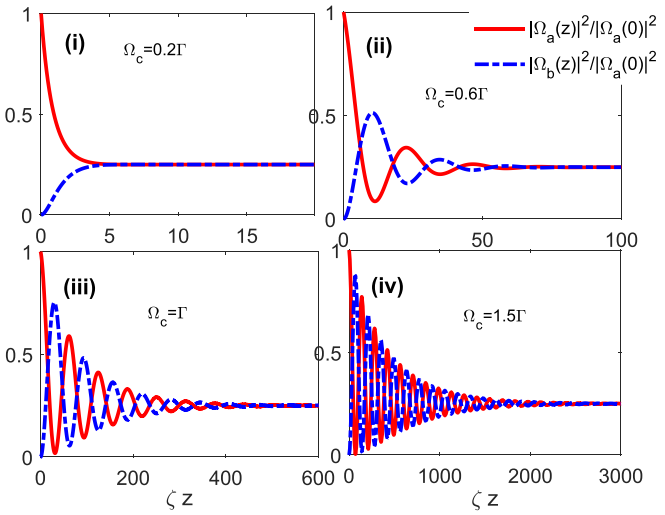

FIG. 4. Dependence of the dimensionless intensities of the light fields $|\Omega_a(z)|^2/|\Omega_a(0)|^2$ (solid line) and $|\Omega_b(z)|^2/|\Omega_a(0)|^2$ (dashed-dotted line) given in Eq. (13) on the distance ζz for (i) $\Omega_c = 0.2\Gamma$, (ii) $\Omega_c = 0.6\Gamma$, (iii) $\Omega_c = \Gamma$, and (iv) $\Omega_c = 1.5\Gamma$. Here, $\theta = \pi/4$, $\Delta = 0.1\Gamma$, $\Delta_c = 0$, and the rest of the parameters are the same as Fig. 2.

and facilitate vortex transfer. Secondly, maintaining a small value for the two-photon detuning is crucial to ensure that the model operates within the slow light regime while minimizing absorption losses. As observed in Figs. 2(ii) and 2(iv), the system exhibits minimal absorption losses at $\Delta = 0.1\Gamma$ due to its proximity to the EIT regime (zero probe detuning). Additionally, the positive slope of the dispersion curve in this vicinity of resonance detuning implies the excellent performance of slow light, as it is very close to resonance.

When the intensity of the control field is relatively weak—specifically, $\Omega_c = 0.2\Gamma$—we observe a pronounced dominance of the imaginary component within the $\wp$. This dominance is reflected in both the initial and subsequently generated vortex fields, which exhibit a gradual exponential relaxation. As propagation ensues, they progressively converge towards a stable state with a value of $1/4$, as illustrated in Fig. 4(i). During this phase, the spatial evolution of the slow light vortices exhibits a smooth and well-matched pattern. Upon intensifying the control field to $\Omega_c = 0.6\Gamma$ [Fig. 4(ii)], and even further to $\Omega_c = \Gamma$ [Fig. 4(iii)], both the imaginary and real components of $\wp$ come into play. Consequently, the behavior of the vortices becomes more complex, displaying a combination of oscillatory and exponential tendencies. Notably, as the intensity of the control field increases, the propagation distance required for the beams to reach their relaxed states also extends. As we continue to increase the intensity of the control field, for instance, to $\Omega_c = 1.5\Gamma$, the dominance shifts toward the real component of $\wp$. This shift results in a highly oscillatory evolution of the vortices, necessitating significantly longer propagation distances to achieve a pulse matching of the slow light vortices. This intricate behavior is illustrated in Fig. 4(iv).

This way, the proposed tripod scheme for the vortex transfer can be utilized in two modes: the oscillation and steady-state modes. In an application or experiment, one needs to produce two vortices with a controllable ratio, and has the ability to set the experimental parameters of optical density (OD) of the medium and the coupling power precisely. Then, the oscillation mode will be applied. In the oscillation mode, the two vortex beams have various combinations, such as 99/1, 90/10, 80/20, . . . , 50/50, ... , 10/90, or 1/99, as demonstrated by the first half cycle of the oscillation in Fig. 4(iii) or 4(iv) (an illustrative example is the "spinor slow light" [52]). In another application or experiment, one needs to produce twin vortices, and has no degree of freedom to vary the experimental parameters. Then, the steady-state mode will be applied. In the steady-state mode, the two vortex beams have exactly the same amplitude independent of any experimental parameter as demonstrated by the steady-state value in Fig. 4(i) or 4(ii).

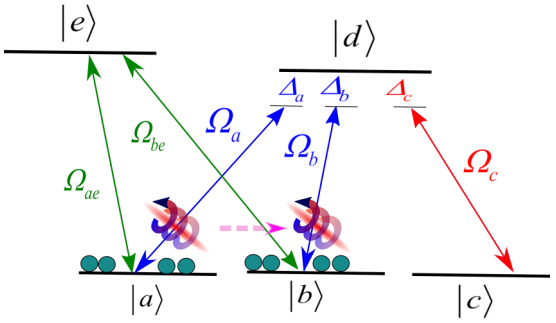

FIG. 5. The level structure of a five-level combined tripod and Λ-type atom-light coupling scheme.

The fundamental premise underpinning the slow light vortex transfer elucidated in this study is encapsulated by Eq. (6), wherein the initial state of the tripod system comprises a superposition of two lower levels, namely, $|a\rangle$ and $|b\rangle$. To model the generation of such coherence between states $|a\rangle$ and $|b\rangle$, we consider a scenario where the tripod scheme, as depicted in Fig. 1, is coupled to an excited state $|e\rangle$ through two resonant and strong control fields Ω_{ae} and Ω_{be}, effectively creating a combined tripod and Λ scheme [17] (see Fig. 5). In this case, both strong fields Ω_{ae} and Ω_{be} act on the Λ subsystem, establishing coherence between states $|a\rangle$ and $|b\rangle$ through the CPT, and preparing the atoms in a CPT (dark) state as described by Eq. (6). The mixing angle, denoted as θ, is now controlled by the resonant control fields Ω_{ae} and Ω_{be}, and is defined as

$$\begin{bmatrix}\cos\theta\\ \sin\theta\end{bmatrix} = \frac{1}{\sqrt{|\Omega_{be}|^2 + |\Omega_{ce}|^2}}\begin{bmatrix}\Omega_{be}\\ -\Omega_{ae}\end{bmatrix}. \tag{14}$$

The remaining equations remain the same, with the only difference being the application of the mixing angle defined in Eq. (14) for θ. Once coherence is established using the strong fields Ω_{ae} and Ω_{be}, these fields will be switched off to prevent affecting the tripod system.

The maximum efficiency achieved for the exchange of slow light vortices using the method presented in this article is around 25%, as shown in Fig. 4. Yet, a complete 100% energy conversion between slow light vortices is possible if we make the system's coherent superposition state, as described in Eqs. (6) and (14), position-dependent by using spatially varying profiles of the control fields Ω_{ae} and Ω_{be}. This requires

separate and comprehensive analysis involving investigating the dynamics of slow vortex beam propagation in a way that satisfies adiabaticity conditions within the local frame of the position domain [28,53,54], which is a topic for future research. This extended approach holds the potential to open up avenues for controlling and manipulating the behavior of slow light vortices, thus enabling advanced applications in the realm of optical information processing and communication.

III. CONCLUDING REMARKS

In conclusion, this paper has investigated the propagation of optical vortices of slow light within a four-level tripod atomic light-matter coupling system. By utilizing a higher-intensity control laser beam coupling an initially unoccupied lower state to the excited state and preparing the system in a coherent superposition of two out of the three lower levels, we have demonstrated the emergence of phase-dependent optical effects through closed level transitions. Solving the Maxwell-Schrödinger equations, our analysis has shown that the strong control field can generate an optical vortex of slow light in a specific transition of the tripod system, which was initially absent within the atomic cloud. Furthermore, we have examined the pulse matching of optical vortices at varying propagation distances, considering the intensity of the control field. Additionally, our investigation has extended to a more complex five-level tripod and Λ scheme, where the introduction of two additional strong control fields enables the preparation of the atom in a coherent superposition of two lower levels. These findings highlight the potential for controlling and manipulating optical vortices of slow light in atomic systems, offering opportunities for applications in fields such as quantum information processing and optical communication.

ACKNOWLEDGMENTS

H.R.H. acknowledges support from Grant No. S-LLT-22-2 "Coherent Optical Control of Atomic Systems" by the Lithuanian Council of Research. I.A.Y. acknowledges support from Grant No. 111-2923-M-008-004-MY3 of the Mutual Funds for Scientific Cooperation between Taiwan, Latvia, and Lithuania, and Grant No. 112-2112-M-007-020-MY3 of the National Council of Science and Technology, Taiwan.

[1] L. V. Hau, S. E. Harris, Z. Dutton, and C. H. Behroozi, Light speed reduction to 17 metres per second in an ultracold atomic gas, Nature (London) **397**, 594 (1999).

[2] M. M. Kash, V. A. Sautenkov, A. S. Zibrov, L. Hollberg, G. R. Welch, M. D. Lukin, Y. Rostovtsev, E. S. Fry, and M. O. Scully, Ultraslow group velocity and enhanced nonlinear optical effects in a coherently driven hot atomic gas, Phys. Rev. Lett. **82**, 5229 (1999).

[3] I. Novikova, D. F. Phillips, and R. L. Walsworth, Slow light with integrated gain and large pulse delay, Phys. Rev. Lett. **99**, 173604 (2007).

[4] J. Ruseckas, A. Mekys, and G. Juzeliūnas, Slow polaritons with orbital angular momentum in atomic gases, Phys. Rev. A **83**, 023812 (2011).

[5] Y. Solomons, C. Banerjee, S. Smartsev, J. Friedman, D. Eger, O. Firstenberg, and N. Davidson, Transverse drag of slow light in moving atomic vapor, Opt. Lett. **45**, 3431 (2020).

[6] M. Fleischhauer and M. D. Lukin, Dark-state polaritons in electromagnetically induced transparency, Phys. Rev. Lett. **84**, 5094 (2000).

[7] D. F. Phillips, A. Fleischhauer, A. Mair, R. L. Walsworth, and M. D. Lukin, Storage of light in atomic vapor, Phys. Rev. Lett. **86**, 783 (2001).

[8] A. S. Zibrov, A. B. Matsko, O. Kocharovskaya, Y. V. Rostovtsev, G. R. Welch, and M. O. Scully, Transporting and time reversing light via atomic coherence, Phys. Rev. Lett. **88**, 103601 (2002).

[9] F. Beil, M. Buschbeck, G. Heinze, and T. Halfmann, Light storage in a doped solid enhanced by feedback-controlled pulse shaping, Phys. Rev. A **81**, 053801 (2010).

[10] S. A. Moiseev and B. S. Ham, Quantum manipulation of two-color stationary light: Quantum wavelength conversion, Phys. Rev. A **73**, 033812 (2006).

[11] J. Otterbach, J. Ruseckas, R. G. Unanyan, G. Juzeliūnas, and M. Fleischhauer, Effective magnetic fields for stationary light, Phys. Rev. Lett. **104**, 033903 (2010).

[12] T. Peters, Y.-H. Chen, J.-S. Wang, Y.-W. Lin, and I. A. Yu, Observation of phase variation within stationary light pulses inside a cold atomic medium, Opt. Lett. **35**, 151 (2010).

[13] U.-S. Kim and Y.-H. Kim, Simultaneous trapping of two optical pulses in an atomic ensemble as stationary light pulses, Phys. Rev. Lett. **129**, 093601 (2022).

[14] M. Fleischhauer, A. Imamoglu, and J. P. Marangos, Electromagnetically induced transparency: Optics in coherent media, Rev. Mod. Phys. **77**, 633 (2005).

[15] Y. Wu and X. Yang, Electromagnetically induced transparency in υ-, Λ-, and cascade-type schemes beyond steady-state analysis, Phys. Rev. A **71**, 053806 (2005).

[16] S. E. Harris, Electromagnetically induced transparency, Phys. Today **50**(7), 36 (1997).

[17] H. R. Hamedi, J. Ruseckas, and G. Juzeliunas, Electromagnetically induced transparency and nonlinear pulse propagation in a combined tripod and Λ atom-light coupling scheme, J. Phys. B: At. Mol. Opt. Phys. **50**, 185401 (2017).

[18] K. Honda, D. Akamatsu, M. Arikawa, Y. Yokoi, K. Akiba, S. Nagatsuka, T. Tanimura, A. Furusawa, and M. Kozuma, Storage and retrieval of a squeezed vacuum, Phys. Rev. Lett. **100**, 093601 (2008).

[19] U. Leonhardt and P. Piwnicki, Relativistic effects of light in moving media with extremely low group velocity, Phys. Rev. Lett. **84**, 822 (2000).

[20] P. Öhberg, Slow light and the phase of a Bose-Einstein condensate, Phys. Rev. A **66**, 021603(R) (2002).

[21] L. Allen, M. J. Padgett, and M. Babiker, The orbital angular momentum of light, Prog. Opt. **39**, 291 (1999).

[22] M. Padgett, J. Courtial, and L. Allen, Light's orbital angular momentum, Phys. Today **57**(5), 35 (2004).

[23] M. Babiker, D. L. Andrews, and V. E. Lembessis, Atoms in complex twisted light, J. Opt. **21**, 013001 (2019).
[24] R. Pugatch, M. Shuker, O. Firstenberg, A. Ron, and N. Davidson, Topological stability of stored optical vortices, Phys. Rev. Lett. **98**, 203601 (2007).
[25] D. Moretti, D. Felinto, and J. W. R. Tabosa, Collapses and revivals of stored orbital angular momentum of light in a cold-atom ensemble, Phys. Rev. A **79**, 023825 (2009).
[26] H. R. Hamedi, J. Ruseckas, and G. Juzeliūnas, Exchange of optical vortices using an electromagnetically-induced-transparency–based four-wave-mixing setup, Phys. Rev. A **98**, 013840 (2018).
[27] H. R. Hamedi, J. Ruseckas, E. Paspalakis, and G. Juzeliūnas, Transfer of optical vortices in coherently prepared media, Phys. Rev. A **99**, 033812 (2019).
[28] H. R. Hamedi, E. Paspalakis, G. Žlabys, G. Juzeliūnas, and J. Ruseckas, Complete energy conversion between light beams carrying orbital angular momentum using coherent population trapping for a coherently driven double-Λ atom-light-coupling scheme, Phys. Rev. A **100**, 023811 (2019).
[29] H. R. Hamedi, V. Kudriasov, N. Jia, J. Qian, and G. Juzeliūnas, Ferris wheel patterning of Rydberg atoms using electromagnetically induced transparency with optical vortex fields, Opt. Lett. **46**, 4204 (2021).
[30] H. R. Hamedi, G. Zlabys, V. Ahufinger, T. Halfmann, J. Mompart, and G. Juzeliunas, Spatially strongly confined atomic excitation via a two dimensional stimulated Raman adiabatic passage, Opt. Express **30**, 13915 (2022).
[31] Y. Zhou and Z. Wang, Helical phase steering via four-wave mixing in a closely cycled double-ladder atomic system, J. Appl. Phys. **133**, 173106 (2023).
[32] F. Song, Z. Wang, E. Li, B. Yu, and Z. Huang, Nonreciprocity with structured light using optical pumping in hot atoms, Phys. Rev. Appl. **18**, 024027 (2022).
[33] C. Yu and Z. Wang, Engineering helical phase via four-wave mixing in the ultraslow propagation regime, Phys. Rev. A **103**, 013518 (2021).
[34] J. Chen, Z. Wang, and B. Yu, Spatially dependent hyper-Raman scattering in five-level cold atoms, Opt. Express **29**, 10914 (2021).
[35] N. S. Mallick and T. N. Dey, Four-wave mixing-based orbital angular momentum translation, J. Opt. Soc. Am. B **37**, 1857 (2020).
[36] S. Sharma and T. N. Dey, Phase-induced transparency-mediated structured-beam generation in a closed-loop tripod configuration, Phys. Rev. A **96**, 033811 (2017).
[37] S. H. Asadpour, Ziauddin, M. Abbas, and H. R. Hamedi, Exchange of orbital angular momentum of light via noise-induced coherence, Phys. Rev. A **105**, 033709 (2022).
[38] Z. A. Sabegh, R. Amiri, and M. Mahmoudi, Spatially dependent atom-photon entanglement, Sci. Rep. **8**, 13840 (2018).
[39] Z. A. Sabegh and M. Mahmoudi, Superluminal light propagation in a normal dispersive medium, Opt. Express **29**, 20463 (2021).
[40] J. Ruseckas, A. Mekys, and G. Juzeliūnas, Optical vortices of slow light using a tripod scheme, J. Opt. **13**, 064013 (2011).
[41] J. Ruseckas, V. Kudriašov, I. A. Yu, and G. Juzeliūnas, Transfer of orbital angular momentum of light using two-component slow light, Phys. Rev. A **87**, 053840 (2013).
[42] H. R. Hamedi, J. Ruseckas, E. Paspalakis, and G. Juzeliūnas, Off-axis optical vortices using double-raman singlet and doublet light-matter schemes, Phys. Rev. A **101**, 063828 (2020).
[43] E. Paspalakis, N. J. Kylstra, and P. L. Knight, Propagation and nonlinear generation dynamics in a coherently prepared four-level system, Phys. Rev. A **65**, 053808 (2002).
[44] E. Paspalakis and Z. Kis, Pulse propagation in a coherently prepared multilevel medium, Phys. Rev. A **66**, 025802 (2002).
[45] P. M. Radmore and P. L. Knight, Population trapping and dispersion in a three-level system, J. Phys. B: At. Mol. Phys. **15**, 561 (1982).
[46] F. T. Hioe and C. E. Carroll, Coherent population trapping in *N*-level quantum systems, Phys. Rev. A **37**, 3000 (1988).
[47] N. V. Vitanov, A. A. Rangelov, B. W. Shore, and K. Bergmann, Stimulated Raman adiabatic passage in physics, chemistry, and beyond, Rev. Mod. Phys. **89**, 015006 (2017).
[48] G. Wang, Y.-S. Wang, E. K. Huang, W. Hung, K.-L. Chao, P.-Y. Wu, Y.-H. Chen, and I. A. Yu, Ultranarrow-bandwidth filter based on a thermal EIT medium, Sci. Rep. **8**, 7959 (2018).
[49] C.-Y. Hsu, Y.-S. Wang, J.-M. Chen, F.-C. Huang, Y.-T. Ke, E. K. Huang, W. Hung, K.-L. Chao, S.-S. Hsiao, Y.-H. Chen, C.-S. Chuu, Y.-C. Chen, Y.-F. Chen, and I. A. Yu, Generation of sub-MHz and spectrally-bright biphotons from hot atomic vapors with a phase mismatch-free scheme, Opt. Express **29**, 4632 (2021).
[50] Y.-F. Chen, P.-C. Kuan, S.-H. Wang, C.-Y. Wang, and I. A. Yu, Manipulating the retrieved frequency and polarization of stored light pulses, Opt. Lett. **31**, 3511 (2006).
[51] J. Ruseckas, G. Juzeliūnas, P. Öhberg, and S. M. Barnett, Polarization rotation of slow light with orbital angular momentum in ultracold atomic gases, Phys. Rev. A **76**, 053822 (2007).
[52] M.-J. Lee, J. Ruseckas, C.-Y. Lee, V. Kudriasov, K.-F. Chang, H.-W. Cho, G. Juzelianas, and I. A. Yu, Experimental demonstration of spinor slow light, Nat. Commun. **5**, 5542 (2014).
[53] Z. Kis and E. Paspalakis, Enhancing nonlinear frequency conversion using spatially dependent coherence, Phys. Rev. A **68**, 043817 (2003).
[54] E. Paspalakis and Z. Kis, Enhanced nonlinear generation in a three-level medium with spatially dependent coherence, Opt. Lett. **27**, 1836 (2002).